International Journal of Mathematical Archive-8(12), 2017, 80-89
Available online through www.ijma.info ISSN 2229 – 5046

MHD BOUNDARY LAYER HEAT AND MASS TRANSFER CHARACTERISTICS OF NANOFLUID OVER A VERTICAL CONE UNDER CONVECTIVE BOUNDARY CONDITION

V. RAMACHANDRA REDDY[1]*, M. SURYANARAYANA REDDY[2]

[1]Research Scholar,
Department of Mathematics, JNTUA, Anathapuramu, (A.P), India.

[2]Assistant Professor,
Department of Mathematics, JNTUACE, Pulivendula, (A.P.), India.

(Received On: 30-10-17; Revised & Accepted On: 21-11-17)

ABSTRACT

This paper investigates the boundary layer flow, heat and mass transfer characteristics over a vertical cone filled with nanofluid saturated porous medium with the influence of magnetic field, thermal radiation and first order chemical reaction subject to the convective boundary condition. Similarity transformation technique is used for the purpose of converting non-linear partial differential equations into the system of complex ordinary differential equations. The computational Finite element method has been employed to solve the flow, heat and mass transfer equations together with boundary conditions. The impact of various pertinent parameters on hydrodynamic, thermal and solutal boundary layers is investigated and the results are displayed graphically. Furthermore, the values of local skin-friction coefficient, rate of temperature and rate of concentration is also calculated and the results are presented graphically. The comparisons with previously published work is made and found good agreement. The thickness of thermal boundary layer is increased with increase in the values of Brownian motion parameter (Nb) and thermophoresis parameter (Nt).

Keywords: *Heat and Mass transfer; Vertical cone; Nanofluid; Convective boundary condition; Finite element method; Chemical reaction.*

NOMENCLATURE

A	Constant
B1	Biot number
B_0	Magnetic field strength
C	Nanoparticle volume fraction
C_f	Skin-friction coefficient
c_p	Specific heat (J/kg K)
C_w	Nanoparticle volume fraction on the cone
C_∞	Ambient nanoparticle volume fraction
Cr	Scaled chemical reaction parameter
D_B	Brownian diffusion coefficient (m^2/s)
D_T	Thermophoretic diffusion coefficient (m^2/s)
g	Gravitational acceleration vector (m/s^2)
J_w	Wall mass flux
k*	Permeability of porous medium
K^*	Mean absorption coefficient
K_m	Thermal conductivity (W m^{-1} K^{-1})
K_r	Chemical reaction parameter
K	Porous parameter
Le	Lewis number
M	Magnetic parameter
Nb	Brownian motion parameter
Nr	Buoyancy ratio parameter
Nt	Thermophoresis parameter
Nu_x	Nusselt number
P	Pressure (Pa)
Pr	Prandtl number
q_r	Radiative heat flux
q_w	Wall heat flux
R	Radiation parameter
Sh_x	Sherwood number
T	Fluid temperature (K)
T_w	Temperature at the cone surface
T_∞	Ambient temperature attained
(u,v)	Velocity components in x- and y-axis (m/s)
(x, y)	Cartesian coordinates

Greek symbols

α	Thermal diffusivity of base fluid (m^2/s)
β	Thermal expansion coefficient (1/K)
σ	Electrical conductivity
σ^*	Stephan-Boltzman constant
ν	Kinematic viscosity of the base fluid (m^2s^{-1})
τ_w	Skin-friction coefficient
ρ_f	Fluid density (kg m^{-3})
ρ_p	Nanoparticle mass density
ψ	Stream function
(ρc_p)	Heat capacitance of the base fluid (J/m^3 K)
τ	Parameter defined by $\varepsilon \frac{(\rho c)_p}{(\rho c)_f}$

Corresponding Author: V. Ramachandra Reddy[1]*
[1]Research Scholar, Department of Mathematics, JNTUA, Anathapuramu, (A.P), India.

$(\rho c_p)_{nf}$	Heat capacitance of the nanofluid
ϕ	Dimensionless nanoparticle volume fraction
θ (η)	Dimensionless temperature

Subscripts

w	Condition at cone surface
∞	Condition far away from cone surface
η	Similarity variable
f	Base fluid

1. INTRODUCTION

Natural convection flow, heat and mass transfer through porous medium over curved bodies is an important area in recent years because of its wide range applications such as chemical engineering, thermal energy storage devices, heat exchangers, ground water systems, electronic cooling, boilers, heat loss from piping, nuclear process systems etc. Spherical geometries, cones, cylinders, ellipses, wavy channels, torus geometries are some examples of curved bodies. Good number of experimental and theoretical studies on transport phenomena over cylindrical bodies has been reported in literature which deals the process of polymer systems. All these studies are mainly focused on flow and heat transfer characteristics of the commonly used base fluids like water, ethylene glycol, oil etc. In recent times, the study of nanofluids has become the topic of extensive research because the presence of nanoparticles would appreciably increase the thermal conductivity of the fluids in heat transfer process. A nanofluid is a fluid containing small volumetric quantities of nanometer-sized (smaller than 100 nm) particles called nanoparticles. Nanofluids are the emerging composites consisting of nanometer size solid particles dispersed in the conventional heat transfer fluids like water, ethylene glycol, toluene, and engine oil. The very key characteristic of nanofluids is their high thermal conductivity relative to the base fluids. The thermal conductivity enhancement of nanofluids has become the most important phenomenon than the limited heat transfer performance of available general fluids. Choi [1] was the first among all who introduced a new type of fluid called nanofluid while doing research on new coolants and cooling technologies. Eastman *et al.* [2] have also exposed in their study that the thermal conductivity has increased 40% when copper nanoparticles of volume fraction less than 1% are added to the ethylene glycol or oil. Buongiorno [3] has developed an analytical model for convective transport in nanofluids, in this study he concluded that there are seven possible mechanisms associating convection of nanofluids through moment of nanoparticles in the base fluid. Tiwari *et al.* [4] have presented heat transfer augmentation of nanofluids in a two-sided lid-driven heated square cavity. Santra *et al.* [5] have reported heat transfer augmentation of copper-water nanofluid in differentially heated square cavity. Abu-nada *et al.* [6] have analyzed natural convection applications of nanofluids over inclined two-dimensional enclosures filled with Cu-water nanofluid. Kuznetsov and Nield [7] studied the influence of Brownian motion and thermophoresis on natural convection boundary layer flow of a nanofluid past a vertical plate. Khan and pop [10] have discussed boundary layer flow, heat and mass transfer of a nanofluid past a stretching sheet. Ghasemi *et al.* [11] have discussed periodic natural convection flow and heat transfer over enclosure filled with nanofluid under the influence of oscillating heat flux. Chamkha *et al.* [12] have discussed the mixed convection flow about vertical cone through porous medium saturated by a nanofluid with thermal radiation. In addition, Gorla *et al.* [13] have studied nanofluid natural convection boundary layer flow through porous medium over a vertical cone. Chamkha *et al.* [14] were presented non-Darcy free convective nanofluid along a vertical plate with suction/injection and internal heat generation. Fernandez-Feria *et al.* [15] have discussed the mixed convection boundary layer radial flow over a horizontal plate with constant temperature. Chamkha *et al.* [16] have investigated Non-Newtonian nanofluid natural convection flow over a cone through porous medium with uniform heat and volume fraction fluxes. Zakari *et al.* [17] have presented the natural convection boundary layer flow, heat and mass transfer analysis of nanofluid influenced by various aspects like, size, shape, type of nanofluid, type of base fluid and working temperature of the base fluid. Ghalambaz *et al.* [18] have reported natural convection flow over a heated vertical plate through nanofluid saturated porous medium. Ghalambaz *et al.* [19] have analyzed natural convection of Al_2O_3- water nanofluid over a vertical cone with the influence of nanoparticles diameter, concentration and variable thermal conductivity. Noghrehabadi *et al.* [20] have noticed the boundary layer natural convection of nanofluid over a vertical plate. Sheremet *et al.* [21] presented Buongiorno's mathematical model of nanofluid over a square cavity through porous medium. Sheremet *et al.* [22] have deliberated three-dimensional natural convection Buongiorno's mathematical model of nanofluid over a porous enclosure. Zargartalebi *et al.* [23] have discussed Stagnation-point natural convection heat and mass transfer flow of nanofluid over a stretching sheet under the variable thermo-physical properties.

Magneto nanofluids have specific applications in biomedicine, optical modulators, magnetic cell separation, magneto-optical wavelength filters, silk float separation, nonlinear optical materials, hyperthermia, optical switches, drug delivery, optical gratings etc. A magnetic nanofluid has both the liquid and magnetic properties. The used magnetic field influences the suspended particles and reorganizes their concentration in the fluid regime which powerfully influences the heat transfer analysis of the flow. Magneto nanofluids are useful to guide the particles up the blood stream to a tumor with magnets. This is due to the fact that the magnetic nanoparticles are regarded more adhesive to tumor cells than non-malignant cells. Such particles absorb more power than microparticles in alternating current magnetic fields tolerable in humans i.e. for cancer therapy. Several authors [24, 25] have discussed the MHD boundary layer flow, heat and mass transfer characteristics of nanofluids.

Generally, natural convection boundary layer flow, heat and mass transfer problems consisting of a heating condition along the boundary of the surface that forms a solid–fluid interface is regularly recommended. The commonly used condition is either a constant temperature or a constant heat flux. In general, there is a question that arises that what surface boundary condition has to be implemented on the surface temperature. Despite the routinely used boundary condition of either constant temperature of constant heat flux, it arises in practice only that when the solid body has more thermal conductivity compared to the porous medium. This is equivalent to say that the Biot number of the problem is not equal to zero, but has a finite value.

Ram Reddy *et al.* [26] examined the mixed convection flow, heat and mass transfer analysis of nanofluid over a vertical plate under convective boundary condition by taking Soret effect into the account. Makinde *et al.* [27] studied analytically the boundary layer flow of nanofluid over a stretching sheet under convective boundary condition. Non-aligned stagnation point flow of nanofluid over a convective stretching sheet with influence of partial slip effect is numerically analyzed by Nadeem *et al.* [28]. Ibanez [29] investigated the entropy generation in a vertical porous channel under convective boundary condition by taking magnetic field and hydrodynamic slip into the account. Hayat *et al.* [30] have reported the impact of magnetic field in three-dimensional flow of couple stress nanofluid over a nonlinearly stretching surface with convective boundary condition.

Although there are good number of publications in the literature on heat and mass transfer characteristics of nanofluids over a vertical cone, to the best of author's knowledge, no studies have been reported that considered convective boundary condition and first order chemical reaction. The objective of present study is, therefore, to investigate numerically the impact of key parameters such as magnetic field, thermal radiation and first order chemical reaction on natural convection flow, heat and mass transfer analysis over a vertical cone through nanofluid saturated porous medium under convective boundary condition.

2. MATHEMATICAL ANALYSIS

Fig.1 demonstrates a two-dimensional, study, electrically conducting heat and mass transfer boundary layer flow of nanofluid over a vertical cone. The coordinate system is chosen as the *x*-axis is coincident with the flow direction over the cone surface. It is assumed that T_w, to be determined, is the result of convective heating process which is characterized by a temperature T_f and a heat transfer coefficient h_f, and C_w is the nanoparticle volume fraction at the surface of the cone ($y = 0$). The temperature and nanoparticle volume fraction of the ambient fluid are T_∞ and C_∞. An external magnetic field of strength B_0 is applied in the direction of the *y*-axis. By considering the work of Kuznetsov et al. [7] in assuming nanoparticle concentration is dilute (that is, no particle-particle interaction exists) and by employing the Oberbeck – Boussinesq approximation the governing equations describing the steady-state conservation of mass, momentum, energy as well as conservation of nanoparticles for nanofluids in the presence of thermal radiation and other important parameters for double diffusive heat and mass transfer conditions take the following form [8,9]:

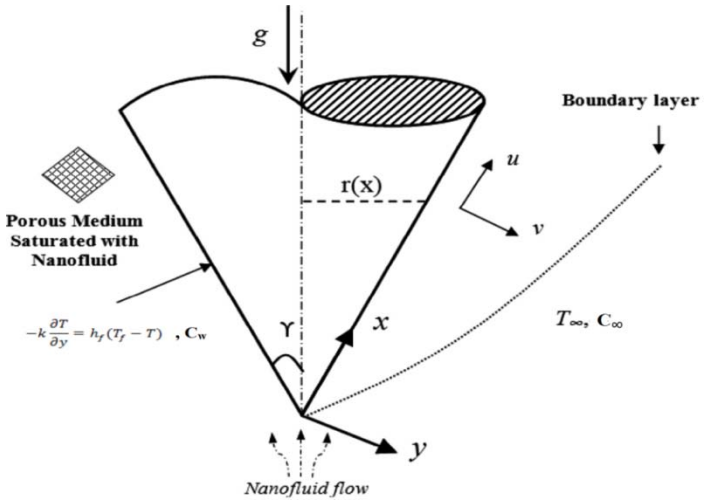

Figure-1: Physical model and coordinate system.

$$\frac{\partial(ru)}{\partial x} + \frac{\partial(rv)}{\partial y} = 0 \tag{1}$$

$$u\frac{\partial u}{\partial x} + v\frac{\partial u}{\partial y} = \nu\frac{\partial^2 u}{\partial y^2} - \frac{\mu}{k^*}u + g\left[(1 - C_\infty)\rho_{f\infty}\beta(T - T_\infty) - (\rho_p - \rho_{f\infty})(C - C_\infty)\right]Cos\gamma - \frac{\sigma {B_0}^2}{\rho_f}u \tag{2}$$

$$u\frac{\partial T}{\partial x} + v\frac{\partial T}{\partial y} = \alpha\frac{\partial^2 T}{\partial y^2} + \tau\left[D_B\frac{\partial C}{\partial y}.\frac{\partial T}{\partial y} + \left(\frac{D_T}{T_\infty}\right)\left(\frac{\partial T}{\partial y}\right)^2\right] - \frac{1}{\rho c_p}\frac{\partial q_r}{\partial y} \tag{3}$$

$$u\frac{\partial C}{\partial x} + v\frac{\partial C}{\partial y} = D_B\frac{\partial^2 C}{\partial y^2} + \left(\frac{D_T}{T_\infty}\right)\frac{\partial^2 T}{\partial y^2} - K_r(C - C_\infty) \tag{4}$$

The associated boundary conditions are

$$u = 0,\ v = 0,\ -k\frac{\partial T}{\partial y} = h_f(T_f - T), \qquad C = C_w \quad at\ y = 0 \tag{5}$$

$$u \to 0, \qquad T \longrightarrow T_\infty, \qquad C \longrightarrow C_\infty \qquad at\ y \to \infty \tag{6}$$

where *u* and *v* denote the components in the *x* – and y – directions, respectively. In the momentum equation (2), the second term on the right hand side is the porous medium term, the third term is the combination of thermal and species buoyancy term and the last term is the hydromagnetic drag term. In the temperature equation (3), the second term on the right hand side is related to Brownian motion and thermophoresis, the third term is the thermal radiation term.

In the diffusion equation (4), the last term corresponds to first order chemical reaction.

The radiative heat flux q_r (using Rosseland approximation) is defined as

$$q_r = -\frac{4\sigma^*}{3K^*}\frac{\partial T^4}{\partial y}, \tag{7}$$

We assume that the temperature variances inside the flow are such that the term T^4 can be represented as linear function of temperature. This is accomplished by expanding T^4 in a Taylor series about a free stream temperature T_∞ as follows:

$$T^4 = {T_\infty}^4 + 4{T_\infty}^3(T - T_\infty) + 6{T_\infty}^2(T - T_\infty)^2 + \cdots$$

After neglecting higher-order terms in the above equation beyond the first degree term in $(T - T_\infty)$, we get

$$T^4 \cong 4{T_\infty}^3 T - 3{T_\infty}^4 \tag{8}$$

Thus substituting Eq. (8) in Eq. (7), we get

$$q_r = -\frac{16{T_\infty}^3\sigma^*}{3K^*}\frac{\partial T}{\partial y} \tag{9}$$

We now introduce the following similarity variables [27] to transform the governing equations into system of ordinary differential equations:

$$\eta = \frac{y}{x}Ra_x^{1/4},\ f(\eta) = \frac{\psi}{\alpha\, Ra_x^{1/4}}, \quad \theta(\eta) = \frac{T - T_\infty}{T_f - T_\infty}, \quad \phi(\eta) = \frac{C - C_\infty}{C_w - C_\infty} \tag{10}$$

where, $Ra_x = \frac{g\beta\rho_{f\infty}(T_w - T_\infty)(1 - C_\infty)cos\gamma x^3}{\mu\,\alpha}$, is the Rayleigh number.

Here, ' *r* ' can be approximated by the local radius of the cone, if the thermal boundary layer is thin, and is related to the *x* coordinate by $r = x\,sin\gamma$.

Substituting Eqs. (9)-(10) into Eqns. (1) - (4), we get the following system of non-linear ordinary differential equations

$$f''' - (f')^2 + ff'' + (\theta - Nr\,\phi) - (M + K)f' = 0 \tag{11}$$

$$(1 + R)\theta'' + Pr\,f\,\theta' + Nb\,\theta'\phi' + Nt(\theta')^2 = 0 \tag{12}$$

$$\phi'' + Le\,f\,\phi' - Le.Cr.\phi + \frac{Nt}{Nb}\,\theta'' = 0 \tag{13}$$

The transformed boundary conditions are

$$\eta = 0, \quad f = 0,\ f' = 1,\ \theta'(0) = -B1\big(1 - \theta(0)\big),\ \phi = 1.$$

$$\eta \longrightarrow \infty, \quad f' = 0, \quad \theta = 0, \quad \phi = 0. \tag{14}$$

where prime denotes differentiation with respect to η, and the significant thermophysical parameters dictating the flow dynamics are defined by

$$Nr = \frac{(\rho_p - \rho_{f\infty})(C_w - C_\infty)}{\rho_{f\infty}\beta(T_w - T_\infty)(1 - C_\infty)}, \qquad Nb = \frac{\tau D_B(C_w - C_\infty)}{\alpha}, \qquad Nt = \frac{\tau D_T(T_w - T_\infty)}{\alpha T_\infty}, K = \frac{x^2}{k^*\,Ra_x^{1/2}}$$

$$Le = \frac{\nu}{D_B},\ Cr = \frac{K_r}{a},\ Pr = \frac{\nu}{\alpha},\ R = \frac{16{T_\infty}^3\sigma^*}{3K^*k},\ M = \frac{\sigma\beta_0^2 x}{\rho Ra_x^{\frac{1}{2}}}, B1 = \frac{h_f x}{k\,Ra_x^{\frac{1}{2}}}. \tag{15}$$

Quantities of practical interest in this problem are the skin-friction coefficient C_f, local Nusselt number Nu_x, and the local Sherwood number Sh_x, which are defined as

$$C_f = \frac{2\,\tau_w}{\rho}, \quad Nu_x = \frac{xq_w}{k(T_w - T_\infty)}, \quad Sh_x = \frac{xJ_w}{D_B(C_w - C_\infty)} \tag{16}$$

Where, τ_w , q_w and J_w are the skin-friction, heat flux and mass flux at the surface and these quantities are, respectively, defined as

$$\tau_w = \mu\left(\frac{\partial u}{\partial y}\right)_{y=0}, q_w = -k\left(\frac{\partial T}{\partial y}\right)_{y=0}, J_w = -D_B\left(\frac{\partial C}{\partial y}\right)_{y=0} \tag{17}$$

Using (16) and (17), the dimensionless skin-friction coefficient, wall heat and mass transfer rates are defined as

$$C_f = 2Ra_x^{\frac{3}{4}}f''(0), \quad Nu_x = -Ra_x^{\frac{1}{4}}\theta'(0), \quad Sh_x = -Ra_x^{\frac{1}{4}}\phi'(0) \tag{18}$$

The set of ordinary differential equations (11) – (13) are highly non-linear, and therefore cannot be solved analytically. The finite-element method [31, 32] has been implemented to solve these non-linear equations.

3. NUMERICAL METHOD OF SOLUTION

3.1. The finite-element method

The finite-element method (FEM) is such a powerful method for solving ordinary differential equations and partial differential equations. The basic idea of this method is dividing the whole domain into smaller elements of finite dimensions called finite elements. This method is such a good numerical method in modern engineering analysis, and it can be applied for solving integral equations including heat transfer, fluid mechanics, chemical processing, electrical systems, and many other fields. The steps involved in the finite-element method are as follows.

(i) *Finite-element discretization*
(ii) *Generation of the element equations*
(iii) *Assembly of element equations*
(iv) *Imposition of boundary conditions*
(v) *Solution of assembled equations*

The assembled equations so obtained can be solved by any of the numerical techniques, namely, the Gauss elimination method, LU decomposition method, etc. An important consideration is that of the shape functions which are employed to approximate actual functions.

4. RESULTS AND DISCUSSION

Comprehensive numerical computations are conducted for different values of the non-dimensional parameters, such as, Magnetic parameter (*M*), Porous parameter (*K*), Buoyancy ratio parameter (*Nr*), Prandtl number (*Pr*), radiation parameter (*R*), Brownian motion parameter (*Nb*), Thermophoresis (*Nt*), Lewis number (*Le*), Biot number (*B1*), Chemical reaction parameter (*Cr*) and the results are illustrated graphically from Figs. 2 – 15. Comparison with previously published work is made and is shown in table 1. The influence of magnetic field parameter (*M*) on velocity, temperature and concentration profiles in the boundary layer is depicted in Figs. 2 - 4. It is noticed from these figures that the hydrodynamic boundary layer thickness decelerates whereas thermal boundary layer thickness and solutal boundary layer thickness heightens with enhance in the values of (*M*). The concentration profiles increases with higher values of *M* (Fig. 4). Figures 5 - 6 illustrate the effect of buoyancy ratio parameter (*Nr*) on velocity and temperature profiles in the boundary layer region. It is observed from fig. 5 that the thickness of hydrodynamic boundary layer is reduced with the enhancing values of buoyancy ratio parameter (*Nr*). The temperature profiles of the fluid increases with increasing values of buoyancy ratio parameter (*Nr*). This is from the reality that higher the values of buoyancy ratio parameter enhance the fluids temperature, so that thermal boundary layer thickness is increased (Fig. 6). The effect of thermal radiation parameter (*R*) on velocity and temperature profiles is shown in Figs. 7 - 8. It is noticed form figures 8, 9 that, the hydrodynamic and thermal boundary layer thickness is enhanced with the higher values of (*R*) in the entire flow region. This is due to the fact that, imposing thermal radiation in the boundary layer region heats up the fluid, which causes an increment in the velocity and temperature of the fluid. Variation of non-dimensional temperature and concentration distributions for different values of thermophoretic parameter (*Nt*) is depicted in Figs 9 to 10. It is noticed that both temperature and concentration profiles elevates in the boundary layer region for the higher values of thermophoretic parameter (*Nt*). The effect of Brownian motion parameter (*Nb*) on temperature profiles is illustrated in Fig. 11. It is noticed that, with the increasing values of Brownian motion parameter (*Nb*), the temperature profiles enhanced (Fig 11) in the boundary layer regime. Figures 13 and 14 depict the influence of Biot number (*B1*) on thermal and solutal boundary layers. It is noticed that the temperature profiles elevates in the entire fluid regime as the values of Biot number (*B1*) increases (Fig. 12). The concentration profiles escalate throughout the fluid regime as the values of Biot number (*B1*) values improves. This is due to the fact that as the values of Biot number (*B1*) increases there is enhancement in the thickness of the solutal boundary layer (Fig.13). The impact of the Lewis number (*Le*) on concentration profiles is plotted in Fig 14. It is observed that concentration distributions decelerate with the increasing values of the Lewis number in the entire boundary layer region. Fig. 15 depicts the variations in concentration distributions in the boundary layer region for different values of chemical reaction parameter (*Cr*). We see from this figure that the concentration profiles are highly influenced and are decelerated with the higher values of chemical reaction parameter. The values of skin-friction coefficient $-f''(0)$, Nusselt number $-\theta'(0)$ and Sherwood number $-\phi'(0)$ are calculated for diverse values of the key parameters entered into the problem when the cone surface is hot and are shown in Table 2. It is evident that skin friction coefficient enhances, whereas the Nusselt number and Sherwood number decelerates with the increasing values of magnetic parameters (*M*). It is also seen from this table that the skin friction coefficient and rates of dimensionless heat transfer decreases whereas dimensionless mass transfer rate elevates with the higher values of (*R*). It is evident from this table that skin friction coefficient is enhanced with the increasing values of thermophoresis parameter (*Nt*). However, Nusselt number and Sherwood number decelerates with an increment in the values of (*Nt*). With the higher values of Brownian motion parameter (*Nb*) the rate of change of velocity and rate of heat transfer decelerates whereas rate of mass transfer enhances in the boundary layer regime. It is observed from this table that both skin friction coefficient and Nusselt number diminishes while Sherwood number enhances with the improving values of chemical reaction parameter (*Cr*). As the values of Biot number (*B1*) increases the rate of velocity and the rate of concentration decelerates whereas rates of heat transfer heightens in the fluid regime.

5. CONCLUSION

In this present study, we have numerically examined the electrically conducting natural convection nanofluid boundary layer flow of heat and mass transfer along a vertical cone with thermal radiation and chemical reaction. The important results of the present study can be summarized as follows.

i) Both temperature and concentration profiles are elevated with the improving values of thermophoresis parameter (*Nt*).
ii) The thickness of thermal boundary layer is amplified, whereas, solutal boundary layer thickness is depreciated with the higher values of Brownian motion parameter (*Nb*).
iii) Increasing the values of Biot number (*B1*) heightens the temperature and concentration of the fluid in the boundary layer regime.

REFERENCES

1. S.U.S. Choi, Enhancing thermal conductivity of fluids with nanoparticles, developments and applications of non-Newtonian flows, in: D.A. Siginer, H.P. Wang (Eds.), FED-Vol. 231/MD, The American Society of Mechanical Engineers 66**,** (1995) 99-105.
2. J.A. Eastman, S.U.S. Choi, S. Li, W. Yu, and L.J. Thompson, Anomalously increased effective thermal conductivities of ethylene glycol-based nanofluids containing copper nanoparticles, Appl. Phys. Lett. 78, (2001) 718-720.
3. J. Buongiorno, Convective transport in nanofluids, J Heat Transfer 128, (2006) 240-250.
4. R.K. Tiwari, and M.K. Das, Heat transfer augmentation in a two-sided lid-driven differentially heated square cavity utilizing nanofluids, Int. J. Heat Mass Transf. 50, (2007) 2002-2018.
5. A.K. Santra, S. Sen, and N. Chakraborty, Study of heat transfer augmentation in a differentially heated square cavity using copper-water nanofluid, Int. J. Therm. Sci. 47, (2008) 1113-1122.
6. E. Abu-Nada, and H.F. Oztop, Effects of inclination angle on natural convection in enclosures filled with Cu-water nanofluid, Int. J. Heat Fluid Flow 30,(2009) 669-678.
7. A.V. Kuznetsov, and D.A. Nield, Natural convection boundary-layer of a nanofluid past a vertical plate, Int. J. Therm. Sci. 49, (2010) 243-247.
8. A.J. Chamkha, A.M. Rashad and H. Al-Mudhaf, Heat and Mass Transfer from Truncated Cones with Variable Wall Temperature and Concentration in the Presence of Chemical Reaction Effects, International Journal for Numerical Methods in Heat and Fluid Flow 22, (2012) 357- .
9. R.S.R. Gorla, A.J. Chamkha and A. Rashad, Mixed Convective Boundary Layer Flow over a Vertical Wedge Embedded in a Porous Medium Saturated with a Nanofluid: Natural Convection Dominated Regime, Nanoscale Research Letters 6, 207, (2011).
10. W.A. Khan, and I. Pop, Boundary-layer flow of a nanofluid past a stretching sheet, Int. J. Heat Mass Transfer 53, (2010) 2477 – 2483.
11. B. Ghasemi, and S.M. Aminossadati, Periodic natural convection in a nanofluid-filled enclosure with oscillating heat flux, Int. J. Therm. Sci. 49, (2010) 1-9.
12. A.J. Chamkha, S. Abbasbandy, A.M. Rashad, and K. Vajravelu, Radiation Effects on Mixed Convection about a Cone Embedded in a Porous Medium Filled with a Nanofluid, Meccanica 48, (2013) 275-285.
13. R.S.R. Gorla, A.J. Chamkha, and V. Ghodeswar, Natural Convective Boundary Layer Flow over a Vertical Cone Embedded in a Porous Medium Saturated with a Nanofluid, Journal of Nanofluids 3, (2014) 65-71.
14. A.J. Chamkha, A.M. Rashad, Ch. RamReddy, and P.V.Murthy, Effect of Suction/Injection on Free Convection along a Vertical Plate in a Nanofluid Saturated Non- Darcy Porous Medium with Internal Heat Generation, Indian Journal of Pure and Applied Mathematics 45, (2014) 321-341.
15. R. Fernandez-Feria, C. del Pino and A. Fernández-Gutiérrez, Separation in the mixed convection boundary-layer radial flow over a constant temperature horizontal plate, Phys. Fluids 26, (2014) 103603. Doi.org/ 10.1063/ 1.4898193.
16. A.J. Chamkha, S. Abbasbandy, and A.M. Rashad, Non-Darcy Natural Convection Flow of Non-Newtonian Nanofluid Over a Cone Saturated in a Porous Medium with Uniform Heat and Volume Fraction Fluxes, International Journal of Numerical Methods for Heat and Fluid Flow 25, (2015) 422-437.
17. A. Zaraki, M. Ghalambaz, A.J. Chamkha, Mehdi Ghalambaz, and Danilo De Rossi, Theoretical analysis of natural convection boundary layer heat and mass transfer of nanofluids: Effects of size, shape and type of nanoparticles, type of base fluid and working temperature, Advanced Powder Technology 26, (2015) 935-946.
18. M. Ghalambaz, A. Noghrehabadi, and A. Ghanbarzadeh, Natural convection of nanofluids over a convectively heated vertical plate embedded in a porous medium, Brazilian Journal of Chemical Engineering 31, (2014) 413-427.
19. M. Ghalambaz, A. Behseresht, A. Behseresht, and A.J. Chamkha, Effects of nanoparticles diameter and concentration on natural convection of the Al_2O_3–water nanofluids considering variable thermal conductivity around a vertical cone in porous media, Advanced Powder Technology 26, (2015) 224-235.
20. A. Noghrehabadi, A. Behseresht, and M. Ghalambaz, Natural convection of nanofluid over vertical plate embedded porous medium, Appl. Math. Mech. (English Edition) 34, (2013) 669-686.

21. M.A. Sheremet, and I. Pop, Conjugate natural convection in a square porous cavity filled by a nanofluid using Buongiorno's mathematical model, Int. J. Heat Mass Transfer 79, (2014) 137-145.
22. M.A. Sheremet, and I. Pop, and M.M. Rahman, Three-dimensional natural convection in a porous enclosure filled with a nanofluid using Buongiorno's mathematical model, Int. J. Heat Mass Transfer 82, (2015) 396-405.
23. H. Zargartalebi, M. Ghalambaz, A. Noghrehabadi, and A.J. Chamkha, Stagnation-point heat transfer of nanofluids toward stretching sheets with variable thermo-physical properties, Doi.org/10.1016/ j.apt.2015.02.008.
24. S. Khalili, S. Dinarvand, R. Hosseini, H. Tamim, and I. Pop, Unsteady MHD flow and heat transfer near stagnation point over a stretching/shrinking sheet in porous medium filled with a nanofluid, Chin. Phys. B 23, (2014) 048203.
25. A.J. Chamkha, and A.M. Rashad, Unsteady Heat and Mass Transfer by MHD Mixed Convection Flow from a Rotating Vertical Cone with Chemical Reaction and Soret and Dufour Effects, The Canadian Journal of Chemical Engineering 92, (2014) 758-767.
26. Ch. Ram Reddy, P.V.S.N. Murthy, A.J. Chamkha, and A.M. Rashad, Soret Effect on Mixed Convection Flow in a Nanofluid under Convective Boundary Condition, International Journal of Heat and Mass Transfer 64, (2013) 384-392.
27. O.D. Makinde, and A. Aziz, Boundary layer flow of a nanofluid past a stretching sheet with a convective boundary condition, Int. J. Thermal Sci. 50, (2011) 1326-1332.
28. S. Nadeem, R. Mehmood, and N.S. Akbar, Partial slip effect on non-aligned stagnation point nanofluid over a stretching convective surface Chin. Phys. B 24 (1), (2015) 1-8.
29. G. Ibanez, Entropy generation in MHD porous channel with hydrodynamic slip and convective boundary conditions, Int. J. Heat Mass Transfer 80, (2015) 274-280.
30. Tasawar Hayat, Arsalan Aziz, Taseer Muhammad, and Bashir Ahmad, Influence of magnetic field in three - dimensional flow of couple stress nanofluid over a nonlinearly stretching surface with convective condition, PLOS ONE, 0145332, (2015).
31. P. Sudarsana Reddy, A.J. Chamkha, Soret and Dufour effects on MHD heat and mass transfer flow of a micropolar fluid with thermophoresis particle deposition, Journal of Naval Architechure and Marine Engineering, 13 (2016) 39-50.
32. P. Sudarsana Reddy, A. J. Chamkha, Soret and Dufour Effects on unsteady MHD heat and mass transfer over a stretching sheet with thermophoresis and non-uniform heat generation/absorption, Journal of Applied Fluid Mechanics 9 (2016) 2443-2455.
33. W.A. Khan, O.D. Makinde, Z.H. Khan, Non-aligned MHD stagnation point flow of variable viscosity nanofluids past a stretching sheet with radiative heat, International Journal of Heat and Mass Transfer 96, (2016) 525-534.

Table-1: Comparison of $-\theta'(0)$ and $-\phi'(0)$ for $\gamma = 0$, K = 0, Cr = 0, Pr =10, Le =10, B1= 0.1.

Parameter		$-\theta'(0)$		$-\phi'(0)$	
Nt	Nb	Khan et al. [47]	Present Study	Khan et al. [47]	Present Study
0.1	0.1	0.0929	0.0927	2.2774	2.2772
	0.5	0.0383	0.0385	2.3560	2.3558
0.3	0.1	0.0925	0.0924	2.2238	2.2236
	0.5	0.0269	0.0267	2.4576	2.4574
0.5	0.1	0.0921	0.0920	2.1783	2.1781
	0.5	0.0180	0.0178	2.5435	2.5434

Table-2: The values of skin-friction coefficient $(-f''(0))$, Nusselt number $(-\theta'(0))$ and Sherwood number $(-\phi'(0))$ for different values of M, R, Nt, Nb, Cr, B1.

M	R	Nt	Nb	Cr	B1	$-f''(0)$	$-\theta'(0)$	$-\phi'(0)$
0.1	0.1	0.5	0.5	0.2	1.0	1.018096	0.345231	0.865893
0.4	0.1	0.5	0.5	0.2	1.0	1.151152	0.336060	0.843815
0.7	0.1	0.5	0.5	0.2	1.0	1.271302	0.327735	0.825215
1.0	0.1	0.5	0.5	0.2	1.0	1.381563	0.320125	0.809353
0.5	0.1	0.5	0.5	0.2	1.0	1.156056	0.366095	0.819394
0.5	0.3	0.5	0.5	0.2	1.0	1.133015	0.352332	0.837684
0.5	0.5	0.5	0.5	0.2	1.0	1.112701	0.340290	0.853652
0.5	0.7	0.5	0.5	0.2	1.0	1.094610	0.329638	0.867701
0.5	0.1	0.1	0.5	0.2	1.0	1.103310	0.357303	0.973750
0.5	0.1	0.4	0.5	0.2	1.0	1.110461	0.344572	0.881889
0.5	0.1	0.7	0.5	0.2	1.0	1.118963	0.327352	0.775839
0.5	0.1	1.0	0.5	0.2	1.0	1.126141	0.309957	0.687372
0.5	0.1	0.5	0.3	0.2	1.0	1.148069	0.355102	0.712206
0.5	0.1	0.5	0.6	0.2	1.0	1.100229	0.331956	0.889516
0.5	0.1	0.5	0.9	0.2	1.0	1.069632	0.306079	0.950824
0.5	0.1	0.5	1.2	0.2	1.0	1.043413	0.280130	0.983159
0.5	0.1	0.5	0.5	0.1	1.0	1.111984	0.340345	0.856159
0.5	0.1	0.5	0.5	0.2	1.0	1.100860	0.339526	0.981267
0.5	0.1	0.5	0.5	0.3	1.0	1.091839	0.338801	1.091424
0.5	0.1	0.5	0.5	0.4	1.0	1.084278	0.338154	1.190733
0.5	0.1	0.5	0.5	0.2	0.1	1.293971	0.143738	0.904779
0.5	0.1	0.5	0.5	0.2	0.3	1.251020	0.189296	0.893228
0.5	0.1	0.5	0.5	0.2	0.5	1.217889	0.224976	0.884215
0.5	0.1	0.5	0.5	0.2	0.7	1.191495	0.253669	0.877018

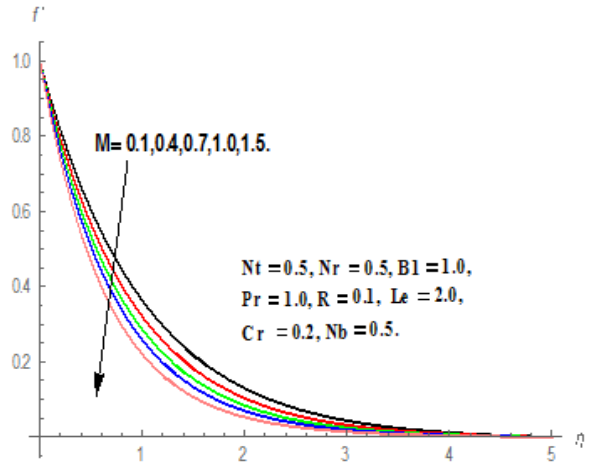

Figure-2: Effect of M on Velocity profile.

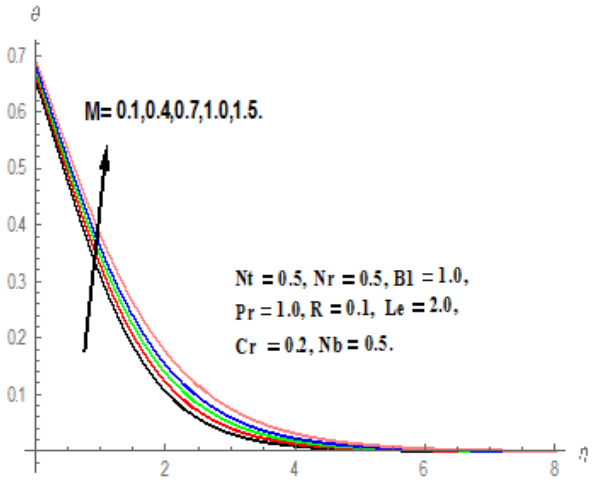

Figure-3: Effect of M on temperature profile.

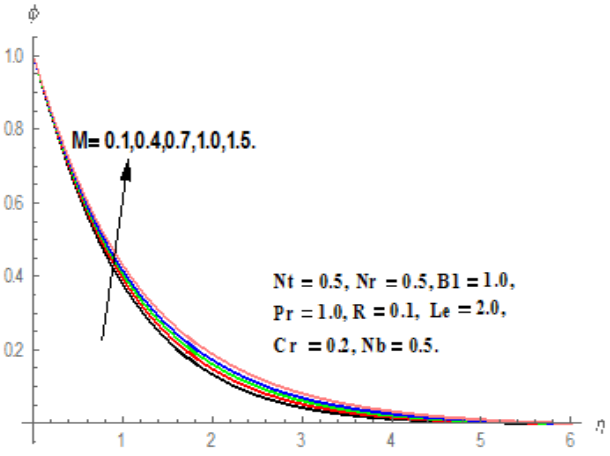

Figure-4: Effect of M on Concentration profile.

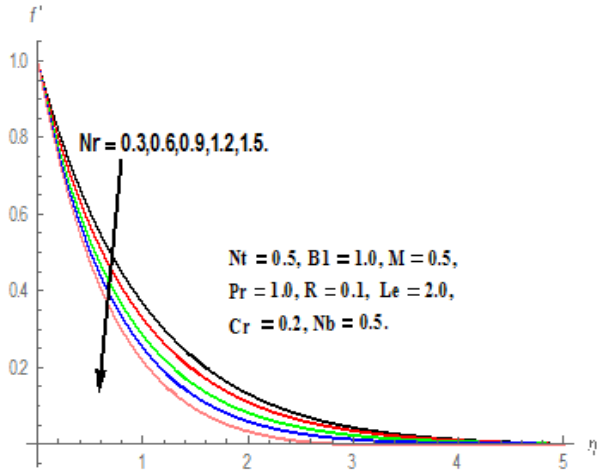

Figure-5: Effect of Nr on Velocity profile.

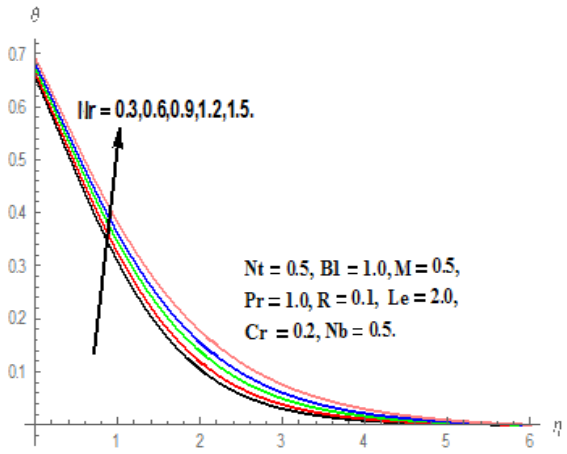

Figure-6: Effect of Nr on Temperature profile.

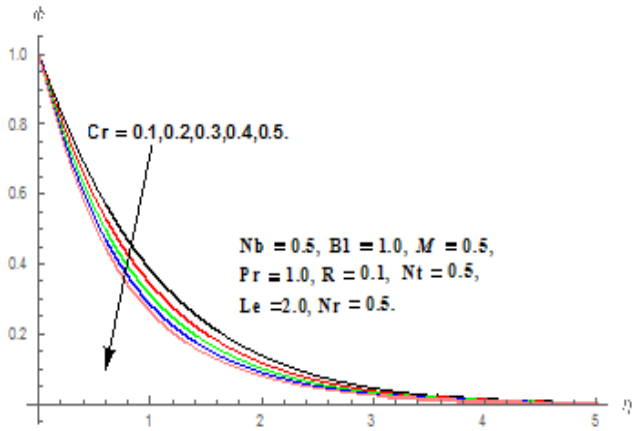

Figure-7: Effect of *Cr* on Concentration profile.

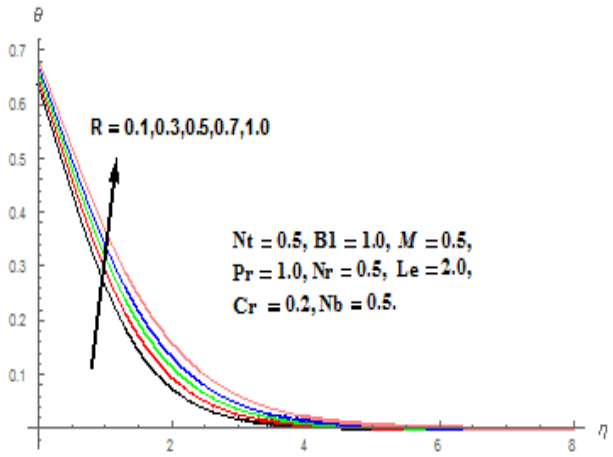

Figure-8: Effect of R on Velocity profile.

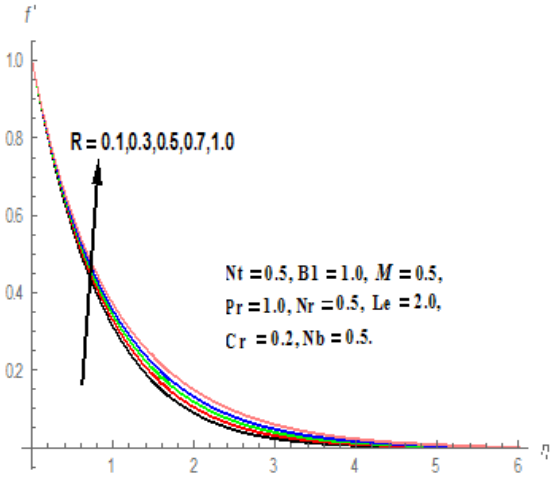

Figure-9: Effect of R on Temperature profile.

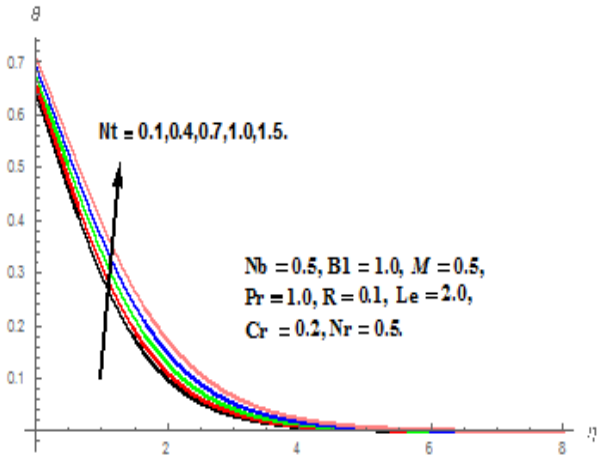

Figure-10: Effect of Nt on Temperature profile.

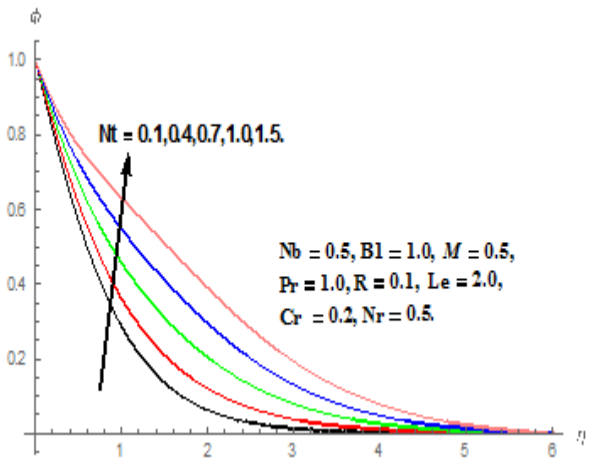

Figure-11: Effect of *Nt* on Concentration profile.

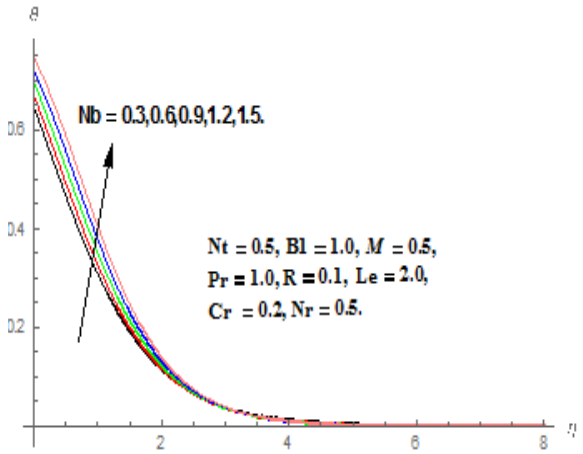

Figure-12: Effect of Nb on Temperature profile.

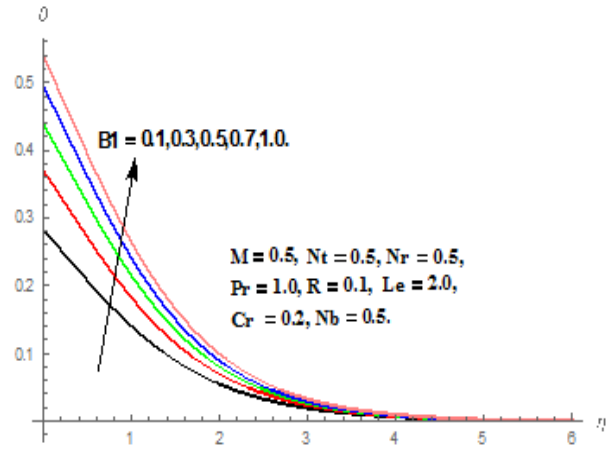

Figure-13: Effect of $B1$ on Temperature profile.

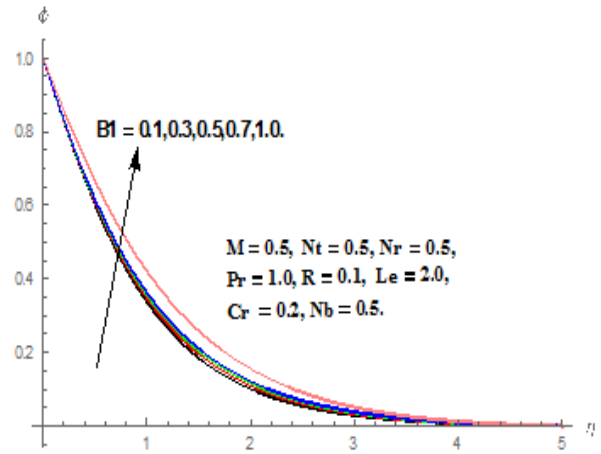

Figure-14: Effect of $B1$ on Concentration profile.

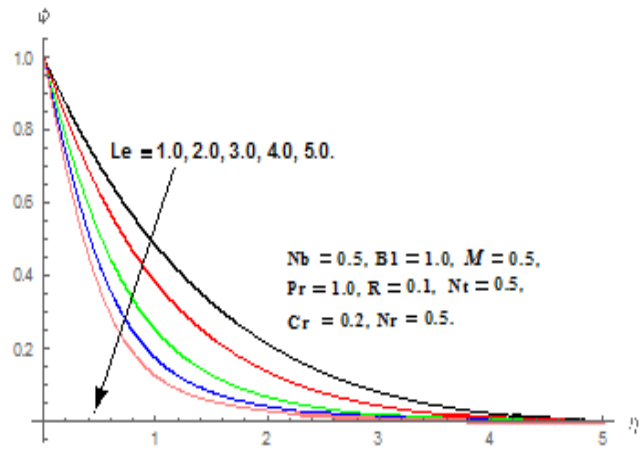

Figure-15: Effect of Le on Concentration profile.

Source of support: Nil, Conflict of interest: None Declared.